Joule Heating Effect on Field-Free Magnetization Switching by Spin-Orbit Torque in Exchange-Biased Systems

Seyed Armin Razavi,[1] Di Wu,[1,2] Guoqiang Yu,[1,*] Yong-Chang Lau,[3] Kin L. Wong,[1] Weihua Zhu,[2] Congli He,[1] Zongzhi Zhang,[2] J. M. D. Coey,[3] Plamen Stamenov,[3] Pedram Khalili Amiri,[1,4] and Kang L. Wang[1]

[1]*Department of Electrical Engineering, University of California, Los Angeles, California 90095-1594, USA*
[2]*Key Laboratory of Micro and Nano Photonic Structures (Ministry of Education), Department of Optical Science and Engineering, Fudan University, Shanghai 200433, People's Republic of China*
[3]*CRANN, AMBER and School of Physics, Trinity College Dublin, Dublin 2, Ireland*
[4]*Inston Inc., Los Angeles, California 90095, USA*

(Received 27 September 2016; revised manuscript received 20 January 2017; published 23 February 2017)

Switching of magnetization via spin-orbit torque provides an efficient alternative for nonvolatile memory and logic devices. However, to achieve deterministic switching of perpendicular magnetization, an external magnetic field collinear with the current is usually required, which makes these devices inappropriate for practical applications. In this work, we examine the current-induced magnetization switching in a perpendicularly magnetized exchange-biased Pt/CoFe/IrMn system. A magnetic field annealing technique is used to introduce in-plane exchange biases, which are quantitatively characterized. Under proper conditions, field-free current-driven switching is achieved. We study the Joule heating effect, and we show how it can decrease the in-plane exchange bias and degrade the field-free switching. Furthermore, we discuss that the exchange-bias training effect can have similar effects.

DOI: 10.1103/PhysRevApplied.7.024023

I. INTRODUCTION

Spin-orbit torque (SOT) switching of magnetization is a promising emerging technology for memory and logic applications [1–3], which offers an advantage over conventional spin-transfer torque in terms of dynamic power dissipation [4–6]. However, to achieve high bit densities, perpendicular magnetization is required [7]. Switching of perpendicular magnetization by SOT has been widely investigated; when an in-plane charge current is passed through a material with high-spin-orbit coupling, such as a heavy-metal layer (Pt [1,3,8], Ta [9–11], W [12], and Hf [13,14]) or even a topological insulator [15], a spin current is generated, and it can apply torques on the adjacent ferromagnetic layer [3,8,16–18]. However, deterministic switching of perpendicular magnetization driven by SOT requires an additional inversion symmetry breaking [19]. Usually, this symmetry is broken by applying an external magnetic field collinear with the current, which is impractical in device applications.

There have been efforts to achieve deterministic switching without the need of an external field. Field-free switching has been achieved by introducing a lateral structural asymmetry, where the thickness of one layer is changed laterally [10,19,20] or by inducing a tilt in the uniaxial anisotropy axis [21]. More recently, field-free switching was realized in the antiferromagnet and ferromagnet systems, where some form of in-plane exchange bias (EB) is used instead of an external field [22–25].

In this work, we use a technique for magnetic field annealing based on current-induced Joule heating and a method for in-plane EB characterization based on measurement of the anomalous Hall effect. With the help of these techniques, we study the field-free switching in the exchange-biased films with the core structure of Pt/CoFe/IrMn. The in-plane EB at the interface of CoFe and IrMn replaces the external field and leads to deterministic field-free switching. By examining the in-plane EB on the device level, we characterize the Joule heating and EB training effects in these structures. We discuss how these effects reduce the in-plane EB field over several switching cycles and, hence, degrade the field-free switching. The results may find potential applications in SOT devices.

II. SAMPLE PREPARATION AND MAGNETIC CHARACTERIZATIONS

The samples consisting of Ta(2)/Pt(3)/CoFe(0.9; 1.1)/IrMn(3)/Pt(1) (thicknesses in nanometers) are grown on Si/SiO_2 substrates by dc magnetron sputtering at room temperature. The samples are patterned into an array of Hall bar devices by standard photolithography and dry-etching techniques. The Hall bars have dimensions of $20 \times 130\ \mu m^2$ and $10 \times 40\ \mu m^2$. These devices are

[*]Corresponding author.
guoqiangyu@ucla.edu

 © 2017 American Physical Society

measured using a Keithley 6221 current source, a Keithley 2182A nanovoltmeter, and a Stanford Research Systems SR830 lock-in amplifier. For low-temperature measurements, we use a physical-properties measurement system. The external magnetic field is generated by an electromagnet driven by a Kepco power supply. All measurements are carried out at room temperature, unless specified. All the magnetic characterizations are done on the device level in order to be more consistent with the rest of the results. The resistance characterizations are carried out using four-probe measurements. Similar results are also obtained in several batches of the same structures.

The current-driven field-free switching mechanism is depicted in Fig. 1(a). A charge current passing through Pt generates a spin current via the spin Hall effect, and the resulting spin current exerts torques on the magnetization of the CoFe layer. The schematic of the measurement is depicted in Fig. 1(b). The magnetic properties characterized by anomalous Hall measurement are shown in Fig. 2. Here, the samples are annealed with an out-of-plane magnetic field of 1 T for 10 min in the $-Z$ direction. Figures 2(a) and 2(b) show anomalous Hall resistance as a function of out-of-plane and in-plane magnetic fields, respectively. In Fig. 2(a), the difference between the resistances of two states is defined by $\Delta R_{\mathrm{field}}$, which represents the total change in perpendicular magnetization measured by the anomalous Hall effect when an out-of-plane external magnetic field is used to switch the magnetization. Perpendicular magnetic anisotropy and out-of-plane EB are present in both samples. The small hysteresis loops in Fig. 2(b) may be a result of misalignment between the external in-plane field and the film's surface. It should also be noted that because of the EB in Fig. 2(b), the samples do not switch between the two stable states along the easy axis, only one of the up or down states is observed. As expected, the sample with $t_{\mathrm{CoFe}} = 0.9$ nm has a larger EB because of its thinner ferromagnetic layer [26]. However, the sample with $t_{\mathrm{CoFe}} = 1.1$ nm switches at lower critical current densities, which should be more appropriate for field-free

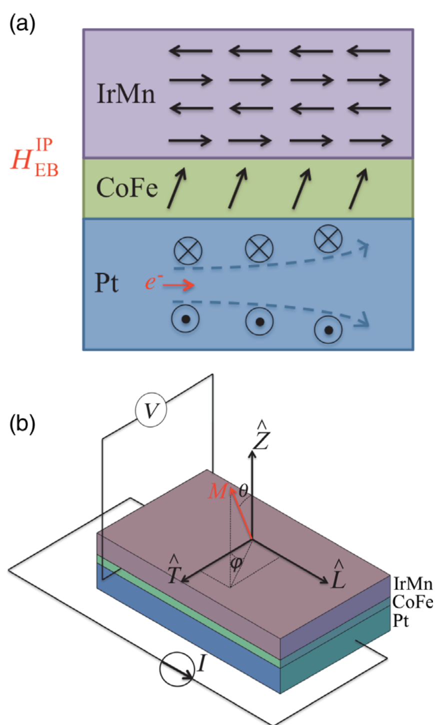

FIG. 1. (a) The studied structure for field-free switching. An antiferromagnet is placed on top of the ferromagnetic layer with perpendicular magnetic anisotropy. A spin current is generated in Pt and exerts torques on the magnetization of the ferromagnetic layer. The in-plane exchange bias $H_{\mathrm{EB}}^{\mathrm{IP}}$ replaces the external field for field-free switching. (b) Schematic of the measurement. I and V show the applied current direction and the measured voltage, respectively. The direction of the exchange-bias field is either out of plane along $\hat{Z}$ or in the longitudinal direction $\hat{L}$. For all the measurements, a Hall bar is used. For current-driven switching measurements, an external magnetic field is applied along the current direction $\hat{L}$. Hall voltage is induced by a current I of constant amplitude 0.5 mA, which is then converted to Hall resistance. M is the magnetization direction, and θ and φ are its polar and azimuthal angles.

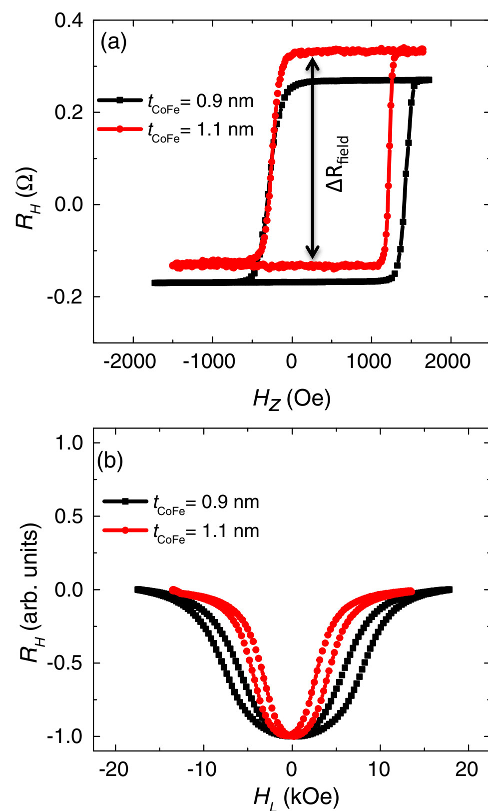

FIG. 2. (a) Perpendicular magnetic anisotropy and out-of-plane exchange bias in samples with $t_{\mathrm{CoFe}} = 0.9$ and 1.1 nm measured by anomalous Hall resistance. The samples are annealed with magnetic field in the $-Z$ direction. (b) Anomalous Hall resistance measured with an in-plane field H_L. The small hysteresis loops are due to slight misalignments between the field and the surface of the samples.

switching since the Joule heating effects are relatively smaller. We also try CoFe layers thinner than 0.9 nm, but as expected, they have even larger critical switching currents and, consequently, a more pronounced Joule heating effect. Furthermore, the samples with CoFe layers thicker than 1.1 nm do not have a good perpendicular magnetic anisotropy and are not useful for the applications. As we discuss in Sec. V, the Joule heating effects are found to degrade the field-free switching; hence, for all the switching measurements, we use the sample with $t_{\mathrm{CoFe}} = 1.1$ nm.

III. CURRENT-DRIVEN MAGNETIZATION SWITCHING WITH OUT-OF-PLANE EXCHANGE BIAS

We first discuss the current-driven switching in the presence of an out-of-plane EB to show the possibility of switching by SOT and to show that out-of-plane EB does not result in field-free switching. A harmonic technique is used to investigate the current-induced SOTs in this case [16,18,27]. It should be noted that in this device, $\xi \equiv \Delta R_P/\Delta R_A = 0.12$, which is the ratio between the planar Hall effect and anomalous Hall effect resistances. To measure ΔR_P (planar Hall effect resistance), a large in-plane field of 1.5 T is applied to the sample to make the magnetization in plane. Then, the transverse resistance is measured as a function of the angle between the in-plane field and the current direction. ΔR_P is defined as the difference between the maximum and the minimum values of the transverse resistance. Furthermore, ΔR_A (anomalous Hall resistance) is defined in the same way as $\Delta R_{\mathrm{field}}$ shown in Fig. 2(a). For the harmonic measurements, a small ac current is passed through the current channel in the presence of an in-plane magnetic field applied along the current (voltage) channel for measuring dampinglike (fieldlike) fields. The ratios corresponding to dampinglike (B_L) and fieldlike (B_T) torques are then calculated [27]

$$B_{L(T)} = -2\left(\frac{\partial V_{2\omega}}{\partial H_{L(T)}}\right)/\left(\frac{\partial^2 V_{\omega}}{\partial H_{L(T)}^2}\right), \tag{1}$$

where V_ω and $V_{2\omega}$ are the first- and second-harmonic anomalous Hall voltage signals, respectively. Figures 3(a)–3(d) show the results for the first- and second-harmonic measurements, which are fitted by parabolic and linear functions, respectively. Finally, we can obtain the dampinglike (ΔH_L) and fieldlike (ΔH_T) fields [27]

$$\Delta H_L = (B_L \pm 2\xi B_T)/(1 - 4\xi^2),$$
$$\Delta H_T = (B_T \pm 2\xi B_L)/(1 - 4\xi^2), \tag{2}$$

where due to our measurement configuration, we use the positive sign in the numerator. Figure 3(e) shows the fieldlike and dampinglike fields at different peak currents. In the small-current regime, the effective fields have a linear dependence on the applied current. Based on the resistances of each layer, the portion of current flowing through the Pt layer is calculated. We estimate that about 47% of the total current passes through the Pt layer. Therefore, the effective dampinglike and fieldlike field efficiencies ($\Delta H_{L(T)}/J$) are calculated to be 22.31 and 7.04 Oe per 10^7 A/(cm)^2, respectively, where J is the peak current density passing through Pt. These values are slightly smaller than other reported values [28,29]. This can be due to the fact that a much smaller portion of the current passes through the IrMn layer, which also generates SOT, and its torques tend to partially cancel the torques from the Pt layer, since they have

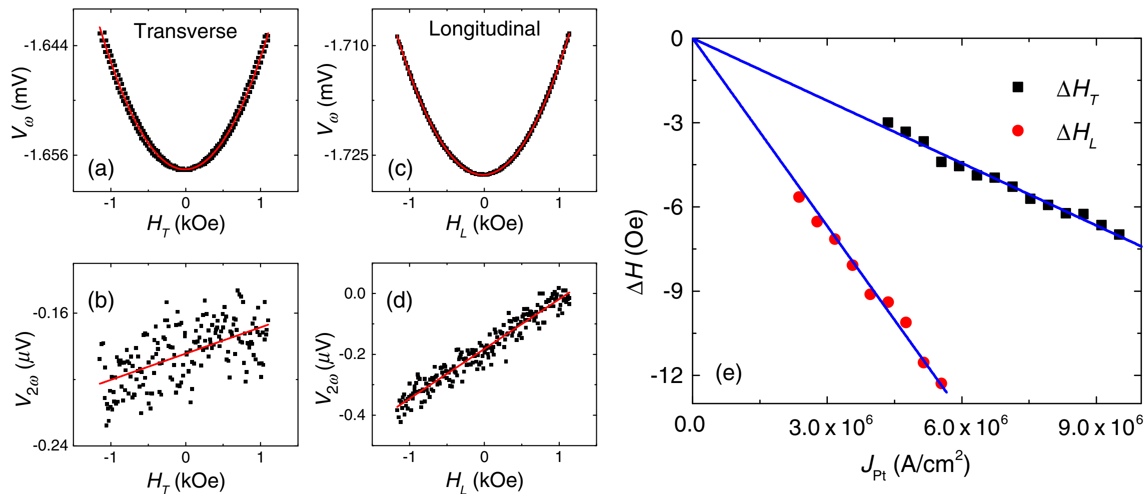

FIG. 3. First- and second-harmonic anomalous Hall voltages for the fieldlike field measurement (a),(b) and dampinglike field measurement (c),(d). H_L and H_T represent the fields applied along the current (longitudinal) and voltage (transverse) channels, respectively. The applied current has an amplitude of 7 mA. (e) Fieldlike and dampinglike field dependence on the peak current density of Pt. The solid line represents the best linear fitting result with zero intercept.

the same sign of the spin Hall angle [30]. It should be noted that the SOT responsible for switching stems from the Pt layer rather than IrMn because of its much higher current density. Assuming that the dampinglike torque is a result of the spin Hall effect solely, we can find the spin Hall angle using $\theta_{\rm SHE} = (-2|e|M_s t_F/h) \times (\Delta H_L/J)$, where $|e|$, h, t_F, and M_s represent the absolute value of the electron's charge, Planck's constant, ferromagnetic layer thickness, and the saturation magnetization of the ferromagnetic layer [31]. Using a superconducting quantum-interference-device measurement, the saturation magnetization is found to be $1100\ \mathrm{emu/cm^3}$. The obtained spin Hall angle for Pt in this structure is 0.082, which is similar to the other reported values for Pt [32].

In order to achieve deterministic switching, we need to break the inversion symmetry; thus, as expected, the out-of-plane EB does not result in field-free switching. Anomalous Hall resistance is used for current-driven switching characterization, and the measurement setup is depicted in Fig. 1(b). For the switching measurement, first an initialization current pulse of +60 mA is applied to the sample. Then, the applied current is swept from +60 to −70 mA and back to +60 mA in the presence of different in-plane magnetic fields, which are collinear with the current direction. To make the switching measurements consistent with the other switching measurements in this work, pulses with 200 μs widths and a 1-s wait between successive pulses are used to drive the magnetization switching.

The resulting plots are shown in Fig. 4. The anomalous Hall resistance is proportional to the perpendicular magnetization; thus, in order to better describe the current-driven switching under different in-plane magnetic fields, we look at the total change in anomalous Hall resistance after sweeping the current. $\Delta R_{\rm field}$ ($\Delta R_{\rm current}$) represents the total perpendicular magnetization reversal when an out-of-plane field (current) is swept. In this case, $\Delta R_{\rm field} = 0.473\ \Omega$. As can be seen in Fig. 4(a), $\Delta R_{\rm current}$ is almost negligible for the zero-field case, which indeed shows that there is no field-free switching. Applying negative and positive in-plane fields results in different switching polarities because of the opposite SOT directions [3]; however, $|\Delta R_{\rm current}|$ is symmetric around the zero field, in other words, there is no shift in the switching diagram, which is reasonable since the EB direction is out of plane. The switching diagram is plotted in Fig. 4(b). The vertical axis shows $\Delta R_{\rm current}/\Delta R_{\rm field}$, which is plotted as a function of different external in-plane magnetic fields H_L. $\Delta R_{\rm current}/\Delta R_{\rm field}$ represents the switching percentage of the sample's area as a result of applying current detected by the anomalous Hall effect. In our notations, $\Delta R_{\rm current}$ has a positive (negative) value if at large positive currents the state with positive (negative) anomalous Hall resistance is preferred. Thus, positive and negative values of $\Delta R_{\rm current}$ correspond to different switching polarities. In this case, we do not have field-free switching; the very small shift in the switching diagram is negligible and may be due to the remanent in-plane field of the magnet.

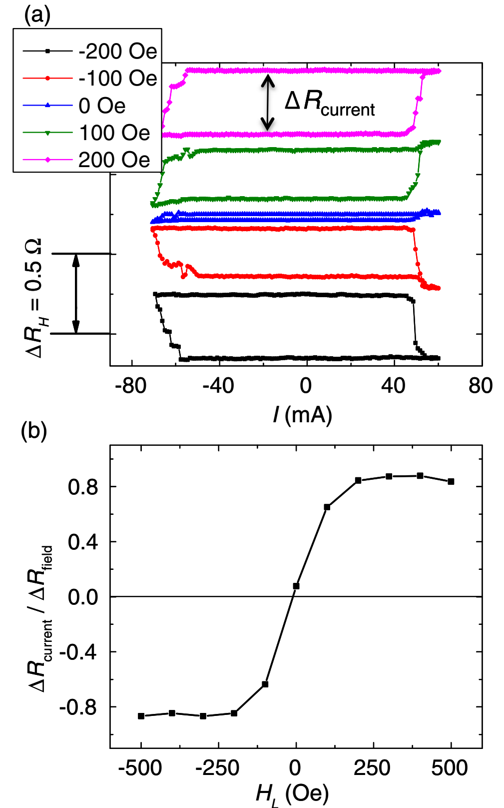

FIG. 4. (a) Current-driven switching in the sample with out-of-plane EB in the presence of different external in-plane magnetic fields H_L. No asymmetry in $|\Delta R_{\rm current}|$ between positive and negative magnetic field values is observed. A current of 45 mA corresponds to a current density of approximately $4 \times 10^7\ \mathrm{A/cm^2}$ passing through the Pt layer. (b) The switching diagram. No shift, or, equivalently, no field-free switching, is observed. Positive and negative values correspond to different switching polarities. For this sample, $\Delta R_{\rm field} = 0.473\ \Omega$.

As can be seen in Fig. 4(b), $\Delta R_{\rm current}$ does not reach $0.473\ \Omega$, even in the presence of larger in-plane magnetic fields. We suppose this is due to the fact that the current density becomes smaller on the Hall bar cross-section area and does not reach the critical value. Furthermore, the additional pinning effect at the cross-section area may make complete switching difficult [30]. Hence, the cross-section region of the device is not completely switched, and $\Delta R_{\rm current}$ does not reach $\Delta R_{\rm field}$.

IV. FIELD-FREE MAGNETIZATION SWITCHING WITH IN-PLANE EXCHANGE BIAS

A. In-plane exchange-bias measurement

For field-free perpendicular magnetization switching, an in-plane EB needs to be introduced. For this purpose, the

sample's temperature should be raised above the blocking temperature in the presence of a large in-plane magnetic field. The blocking temperature is defined as the lowest temperature at which the exchange bias becomes zero [26]. In order to extract the blocking temperature quantitatively, we measure the temperature dependence of the out-of-plane EB. First, the sample is annealed with an out-of-plane field. Then, its temperature is reduced to 100 K in vacuum and in the presence of an out-of-plane field of 1 T. Subsequently, the out-of-plane EB is measured at different temperatures up to 350 K, and by fitting the data, the blocking temperature is found to be around 360 K.

We anneal the devices using current-induced Joule heating in the presence of a large in-plane magnetic field, which can saturate the magnetization. In this technique, a dc current with proper amplitude is applied to the device, which is placed inside a magnetic field. The amplitude of the applied current is large enough to raise the sample's temperature above the blocking temperature but not to burn the device. The appropriate amplitude is found experimentally for each CoFe thickness. The magnetic field is applied along the longitudinal direction of the Hall bar; hence, the longitudinal EB is obtained in the L direction as shown in Fig. 1(b). For the sample with $t_{\mathrm{CoFe}} = 1.1$ nm, we apply 20- and 30-mA dc currents for the 10- and 20-μm Hall bar widths, respectively, which translates to a temperature of 400 K according to the temperature dependence of the resistance in the sample. This temperature is indeed higher than the blocking temperature. This amplitude results in the largest in-plane EB without damaging the structure. The current is applied for 10 min in the presence of an external field of 1.5 T. Then the samples are cooled for 5 min in the air with the magnetic field on. After this procedure, the samples have the same total resistance change $\Delta R_{\mathrm{field}}$ measured by anomalous Hall effect, which suggests that the magnetic properties are not degraded.

In order to measure the in-plane EB field, the anomalous Hall resistance is measured as a function of in-plane external field. The total magnetic energy can be expressed as

$$E = (-K_u + 2\pi M_s^2)\cos^2\theta - M_s(H_T\cos\varphi\sin\theta + H_L\sin\varphi\sin\theta + H_z\cos\theta), \quad (3)$$

where K_u is the magnetic anisotropy, which is in out-of-plane direction, M_s is the saturation magnetization, θ and φ are the polar and azimuthal angles of the magnetization, respectively, and H_T, H_L, and H_z are the transverse, longitudinal, and perpendicular magnetic field components, respectively, as illustrated in Fig. 1(b). It should be noted that here we assume that the magnetization remains uniform in the process. For the in-plane EB measurement, an external field in the longitudinal direction is applied, hence, $\varphi = 90°$. Thus, Eq. (3) can be rewritten as

$$E = (-K_u + 2\pi M_s^2)\cos^2\theta - M_s H'_L\sin\theta, \quad (4)$$

where $H'_L = H_L + H_{\mathrm{EB}}^{\mathrm{IP}}$ should be used instead of H_L to account for the in-plane EB field. Here, we assume that the out-of-plane EB is small and negligible, which can be confirmed by the out-of-plane AHE loop. For different values of external magnetic field, the total energy should be minimized with respect to θ. As a result,

$$\frac{\partial E}{\partial\theta} = (-K_u + 2\pi M_s^2)(-\sin 2\theta) - M_s H'_L\cos\theta = 0. \quad (5)$$

Since H'_L is small compared to the anisotropy field, then $\cos\theta = 0$ is not a physically valid solution. Thus,

$$\sin\theta = \frac{M_s H'_L}{2(K_u - 2\pi M_s^2)} = \alpha H'_L, \quad (6)$$

where $\alpha H'_L$ is very small, and α is a constant for each sample. The anomalous Hall resistance is proportional to the out-of-plane component of the magnetization or $R_H \propto M_z = M\cos\theta = M\sqrt{1-(\alpha H'_L)^2}$, which can be approximated near $\alpha H'_L = 0$ as $R_H \propto M[1-(\alpha^2 {H'_L}^2/2)] = M[1-(\alpha^2/2)(H_L + H_{\mathrm{EB}}^{\mathrm{IP}})^2]$. Consequently, in order to find the EB field, R_H is measured at multiple in-plane magnetic fields around its extremum, then a quadratic function is fitted, and the extremum value is found. The extremum is where $H'_L = H_L + H_{\mathrm{EB}}^{\mathrm{IP}} = 0$, so the EB field can be extracted. This is illustrated in Figs. 5(a) and 5(b). On the same structure as in Sec. III ($t_{\mathrm{CoFe}} = 1.1$ nm), an in-plane EB field is introduced in two opposite directions $\pm\hat{L}$. A small current of 0.5-mA amplitude is used to measure the anomalous Hall resistance, and the EB fields are extracted using the method described above. In this measurement, the in-plane magnetic field is swept back and forth, and each point on the graph represents the average of the two values. The difference of the EB magnitudes for the opposite directions comes from the fact that they are measured on two different devices. However, these devices both have the same structure and are from the same film; thus, this small difference does not affect the validity of the arguments.

This method enables us to quantitatively measure the in-plane EB at different stages in the process. Hence, we are able to do a comprehensive study of the Joule heating and training effects on the in-plane EB and field-free switching, which are discussed in more detail in Sec. V.

B. Field-free magnetization switching

After obtaining large in-plane EB fields, field-free current-driven magnetization switching is achieved, as

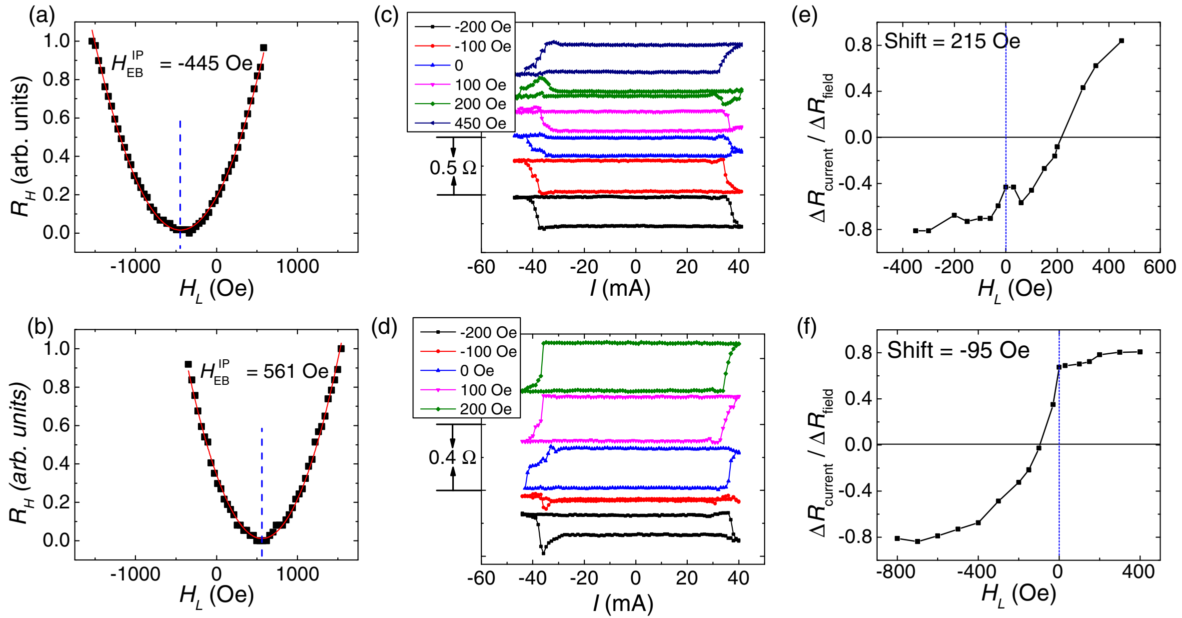

FIG. 5. (a),(b) In-plane exchange-bias field introduction in two different directions. The red line is the quadratic fit; the resulting extremum yields the in-plane exchange-bias field. (c),(d) Current-driven switching with in-plane exchange bias in two different directions measured at different values of applied in-plane field H_L. $|\Delta R_{\mathrm{current}}|$ is, in each case, asymmetric with respect to different fields. Field-free switching is observed. A current of 35 mA corresponds to a current density of approximately $3.1 \times 10^7\ \mathrm{A/cm^2}$ passing through the Pt layer. (e),(f) The switching diagram for different in-plane exchange-bias directions. Shifts to opposite directions are observed, which is consistent with the exchange-bias field directions. It should be noted that (a), (c), and (e) are the results for first direction and (b), (d), and (f) are the results for the second one.

described in the following. The measurement is done as described in Sec. III. Again, for these measurements, a pulsed current is used. The results are depicted in Figs. 5(c) and 5(d), where field-free switching is observed as expected. The field-field switching polarity with positive (negative) EB field is the same as that with positive (negative) external in-plane field, which indicates that the in-plane EB indeed plays the role of the external field. Unlike Fig. 4(a), in this case $|\Delta R_{\mathrm{current}}|$ is asymmetric with respect to different in-plane magnetic fields H_L. We attribute this phenomenon to the presence of in-plane EB. Switching diagrams are plotted in Figs. 5(e) and 5(f). A clear shift in two different directions is observed, which is consistent with the EB field directions for each case. As a result of these shifts, field-free switching is achieved. This can be described very well with the depicted switching diagrams; in these cases, $\Delta R_{\mathrm{current}}$ is large at zero field but vanishes at some other in-plane field, where the EB cancels the external field, and no switching is observed. In these switching diagrams, $\Delta R_{\mathrm{current}}$ and $\Delta R_{\mathrm{field}}$ at zero field are around 50% and 90% of the maximum values, respectively. The maximum value of 0.81 is obtained for an approximately 400-Oe in-plane field.

It should be noted that in both cases, the shift in the switching diagram is smaller than the measured in-plane EB field. As we discuss in more detail in Sec. V, this can be a result of the nonuniformity of the EB field throughout the device [22] or the in-plane EB reduction because of Joule heating or EB training effect [33]. However, this needs further investigation. Furthermore, the amount of shift in Figs. 5(e) and 5(f) is not the same. This may be due to Joule heating or the EB training effect, which can change the in-plane EB during the measurement, and, consequently, the observed shifts in the switching diagrams depend on the sequence in which the measurement is carried out.

V. JOULE HEATING AND EXCHANGE-BIAS TRAINING EFFECTS ON THE FIELD-FREE SWITCHING

A. Joule heating effect

In order to limit the heating effects in the current-driven switching measurements, a pulsed current is used. The critical current for switching is around 40–50 mA, depending on the device dimensions, which translates to a current density of approximately $4 \times 10^7\ \mathrm{A/cm^2}$ passing through the Pt layer. These relatively large amplitudes can increase the sample's temperature through Joule heating. The IrMn thickness of the structure used in the measurements is 3 nm; thus, a low blocking temperature is expected [34].

For a quantitative study of the Joule heating effects, we measure how the temperature of the sample changes in the switching measurement. To that end, we measure how the resistance of the sample changes during the time that the

pulses are applied for switching. We also measure the temperature dependence of resistance, in a range from 110 to 350 K, and we extrapolate the resistance at higher temperatures. By comparing these two sets of data, we estimate the temperature changes during switching. As can be seen in Fig. 6(a), the temperature can rise to 500 K during the switching, which is well above the blocking temperature. This can result in an irreversible loss of the exchange bias.

In order to show the importance of the heating effects in these structures, we compare the field-free switching of a sample under pulsed and dc currents. For the dc current measurement, which is an extreme case in terms of Joule heating, the amplitude of the applied current changes from large negative values to large positive values and back with no delay between consecutive values. Each value is applied for around 200 ms.

For this purpose, a sample with $t_{\mathrm{CoFe}} = 1.1$ nm is annealed using the current. An in-plane EB field of 540 Oe is introduced in the sample. Then the sample is switched using dc current at zero external field. Afterwards, the annealing procedure is repeated to ensure that the in-plane EB field of 540 Oe is still present. This time, the sample is switched at zero external field using pulsed current. The results are shown in Fig. 6(b). With pulsed current, field-free switching is achieved, while with dc current, almost no change in Hall resistance (or, equivalently, in perpendicular magnetization) is observed. We attribute this effect to Joule heating and its impact on the disappearance of the in-plane EB, since the temperature of the sample rises above the blocking temperature during the measurement.

Furthermore, even if pulsed current is used, the field-free switching still degrades after repeating the measurement several times. This can be seen in Fig. 6(c). Here, the field-free switching measurement of the same structure used above is repeated 12 times. The total change in Hall resistance in the switching measurement is decreased, and the field-free switching disappears over the time. This can again be attributed to the Joule heating effect. However, in this case, the EB training effect may also be a contributing factor, and this is discussed in the next section.

With the help of our device-level in-plane EB measurement technique, we observe that after each current-driven field-free switching cycle, the in-plane EB is reduced and eventually it disappears, as depicted in Fig. 7(a). As noted, in the switching measurement, the temperature of the sample goes above the blocking temperature during the pulse application time. On the other hand, the relevant time scale τ for antiferromagnetic reordering is given by [22,35]

$$\frac{1}{\tau} = \nu_0 \exp\left(-\frac{E_b}{k_B T}\right), \tag{7}$$

where $\nu_0 \approx 10^9$ Hz is the attempt frequency, E_b is the energy barrier for antiferromagnetic grain reversal, k_B is Boltzmann's constant, and T is the temperature. For samples with several weeks of stability, τ is around 10^6 s at room temperature (T_0), which results in $E_b \approx 34.5 \times k_B T_0$. The temperature in our measurement goes as high as 500 K, so the corresponding time scale τ is approximately 1 s, which is much longer than the pulse duration of 200 μs. Consequently, the exchange bias does not vanish with one large pulse; it decreases gradually after many pulses. This can also explain why in the dc measurement no field-free switching is observed. In the dc measurement, the high temperature is kept for much longer than 1 s; as a result, the exchange bias vanishes instantly, and no field-free switching is observed. It should be noted that the Joule heating of the 0.1-mA current used for in-plane EB measurement is found to be negligible based on a control measurement in which only the current is applied. In the control measurement, the sample is not switched; only an in-plane field is applied to measure the in-plane EB successively, and after 20 times, there is no significant change in the

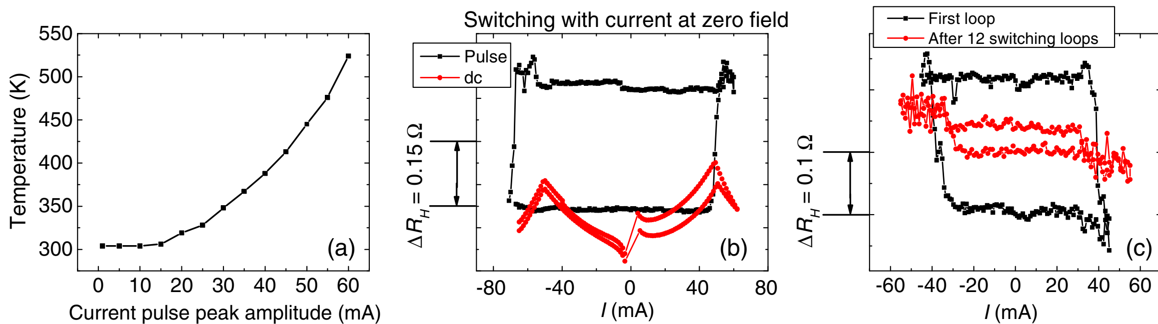

FIG. 6. (a) Temperature change at different current pulse peak amplitudes. (b) Current-driven field-free switching comparison of dc and pulsed currents. With pulse current, field-free switching is achieved, while with dc, almost no change in the Hall resistance is observed. This is attributed to Joule heating effect. (c) The degrading of field-free switching after 12 successive switching measurements. For this purpose, only pulsed current is used, and the same measurement is repeated 12 times. A current of 35 mA corresponds to a current density of approximately 3.1×10^7 A/cm^2 passing through the Pt layer.

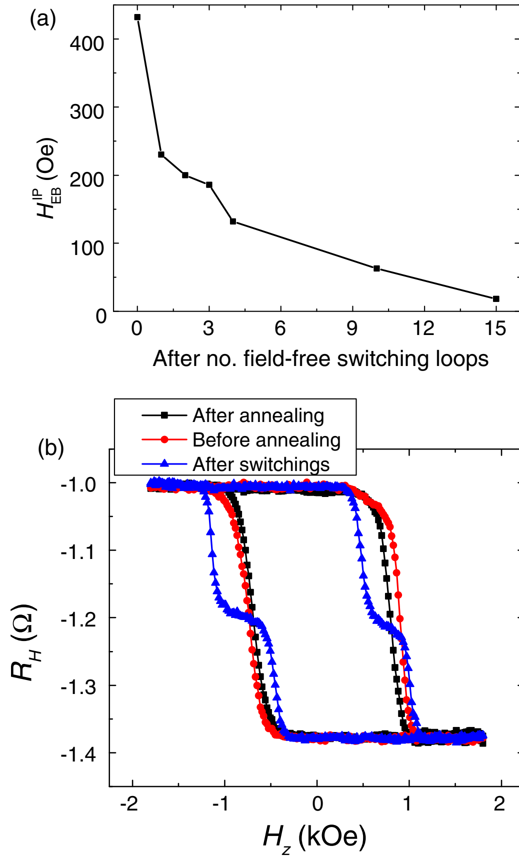

FIG. 7. (a) In-plane exchange-bias change after several field-free current-driven switching cycles. A current of 0.1 mA is used for the exchange-bias measurement. (b) Anomalous Hall measurement with out-of-plane field before and after current annealing with in-plane field and after current-driven switching measurement. Annealing in the presence of in-plane field reduces the out-of-plane exchange bias. After the switching measurement, the out-of-plane exchange bias appears again in the form of double loops.

EB value. This shows that the heating effect of the 0.1-mA current can be neglected.

The disappearance of in-plane EB as a result of heating can be further supported by the comparison of anomalous Hall data, R_H as a function of H_z, at different stages in the process: before and after current annealing with in-plane field and after the current-driven switching measurement shown in Fig. 7(b). After annealing in the presence of a large in-plane magnetic field, the out-of-plane EB decreases, which shows that the pinning is in the in-plane direction. Also, the coercivity is decreased by approximately 100 Oe when the out-of-plane EB decreases, which agrees with other reported findings [36]. After annealing, current is used to switch the sample through 12 cycles, where the critical current for switching is around 45 mA. After current-driven switching measurement, the out-of-plane EB appears again, this time in the form of double loops, which further indicates the presence of heating effects. The temperature of the sample with perpendicular easy axis is raised above the blocking temperature in the course of the switching measurement in the absence of any large external fields. Consequently, the out-of-plane EB tends to appear again, but there is no preference between upward and downward pinning directions because both are along the easy axis, and there is no external field to make a preference. Thus, some parts of the sample have an upward pinning and the other parts have a downward pinning; hence, the double-loop EB appears.

Increasing the IrMn thickness raises the Néel and blocking temperatures; however, that is not desirable since it also increases the shunting effect. The SOT for switching stems from the Pt layer, as shown in Sec. III. By increasing the IrMn thickness, the shunting effect becomes significant and less current passes through Pt. Consequently, the critical current for switching increases. This results in more Joule heating effect and is not desirable. We try samples with thicker IrMn layers up to 10 nm, but field-free switching is not achieved in them.

The Joule heating effect is helpful when switching is assisted with an external in-plane field. In the same sample, using dc current reduces the critical current density for switching by 10% compared to the case where pulsed current is used. That is due to the fact that the Joule heating effect raises the temperature of the sample and reduces the anisotropy, and, consequently, switching becomes easier. On the other hand, when an in-plane EB is used for field-free switching, the heating effect is no longer desirable, since it reduces the in-plane EB field. In this case, avoiding the thermal effect is crucial.

B. Exchange-bias training effect

Even if very short pulses with negligible heating effects are used, the in-plane EB will not be constant after successive switchings due to the EB training effect. The training has mostly been investigated in cases where an external magnetic field is used for cycling through hysteresis loops [33,37,38]. However, it can also exist when SOT is used for magnetization switching. The spin structure at the interface of the antiferromagnet and ferromagnet deviates from its equilibrium state when an EB field is created. Consecutive switchings can result in a rearrangement of the IrMn's spin structure at the interface of IrMn/CoFe towards an equilibrium state [33]. Consequently, a gradual decrease in the in-plane EB is possible. It should be noted that there are also some other models and explanations provided for the origin of the EB training effect [38–43]. However, in this work, we focus only on the general concept.

In order to show this effect in our structure, a sample with $t_{CoFe} = 1.1$ nm is current annealed, and an in-plane EB field of 560 Oe is introduced. Then, an out-of-plane external field is used to switch the sample back and forth. Afterwards, the in-plane EB is measured again and so on.

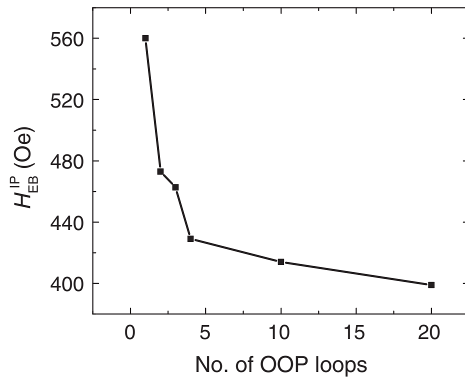

FIG. 8. Training effect of the in-plane exchange bias after successive switching cycles with an out-of-plane field. After each out-of-plane (OOP) loop, the in-plane exchange-bias field is decreased, but it has a saturation value. A current of 0.1 mA is used for the measurements.

The result is depicted in Fig. 8. After each out-of-plane loop, the in-plane EB is decreased, and this can be attributed to the training effect. In our case, SOT is used to switch the perpendicular magnetization. However, as described above, multiple switchings of the magnetization itself result in a reduction of the in-plane EB. This can be a major problem for these devices, since the in-plane EB is essential for field-free switching. As shown in Fig. 8, after only 20 successive switchings, the in-plane EB is reduced by around 30%. This effect will deteriorate the device performance very fast over the time. By comparing the results of Figs. 7 and 8, it can be seen that in our measurements, the Joule heating effect is dominant over the exchange-bias training effect in terms of decreasing the in-plane EB.

VI. CONCLUSION

Field-free perpendicular magnetization switching driven by spin-orbit torque in an asymmetric exchange-biased system of Ta/Pt/CoFe/IrMn/Pt is achieved with the help of device-level magnetic field annealing. The induced in-plane EB plays the role of the external magnetic field required for breaking system symmetry. Through in-plane EB characterization techniques, it is found that Joule heating and exchange bias training effects can significantly affect the field-free switching in these structures. In order to make practical applications possible, these effects are very important issues that need to be addressed. To have more robust field-free switching, very narrow pulses can help with the Joule heating problem, as suggested by the comparison of dc and pulsed currents for switching, where a significant improvement can be seen with pulsed currents. Furthermore, a thin layer inserted between the ferromagnetic and antiferromagnetic layers can help with thermal stability [22]. The training effect is known to be smaller in structures with single-crystalline antiferromagnet layers [26]; thus, that may potentially help with the training-effect problem. Furthermore, as shown in Fig. 8, there is a saturation value for the in-plane EB, which can be high enough to be used for field-free switching. However, the training effect has to be studied in these devices, and they should be designed to have an adequate saturation value.

ACKNOWLEDGMENTS

This work is supported in part by C-SPIN and FAME, two of six centers of STARnet, a Semiconductor Research Corporation program sponsored by MARCO and DARPA. This work is also supported by the National Science Foundation (Grant No. ECCS 1611570) and Nanosystems Engineering Research Center for Translational Applications of Nanoscale Multiferroic Systems Cooperative Agreement Grant No. EEC-1160504. We like to acknowledge the collaboration of this research with the King Abdul-Aziz City for Science and Technology via The Center of Excellence for Green Nanotechnologies. This work is supported as part of the SHINES Center, an Energy Frontier Research Center funded by the U.S. Department of Energy, Office of Science, Basic Energy Sciences under Award No. S000686. D. W. and Z. Z. Z. thank for the support of the China Scholarship Council, the 973 Program (Grant No. 2014CB921104), and the National Natural Science Foundation of China Grant No. 11474067. Y.-C. L., P. S., and J. M. D. C. acknowledge the support by Science Foundation Ireland through AMBER and by Grant No. 13/ERC/I2561. In addition, G. Q. Y. acknowledges Junyang Chen for fruitful discussions.

S. A. R. and D. W. contributed equally to this work.

[1] I. M. Miron, K. Garello, G. Gaudin, P. J. Zermatten, M. V. Costache, S. Auffret, S. Bandiera, B. Rodmacq, A. Schuhl, and P. Gambardella, Perpendicular switching of a single ferromagnetic layer induced by in-plane current injection, Nature (London) **476**, 189 (2011).

[2] L. Liu, C. F. Pai, Y. Li, H. W. Tseng, D. C. Ralph, and R. A. Buhrman, Spin-torque switching with the giant spin Hall effect of tantalum, Science **336**, 555 (2012).

[3] L. Liu, O. J. Lee, T. J. Gudmundsen, D. C. Ralph, and R. A. Buhrman, Current-Induced Switching of Perpendicularly Magnetized Magnetic Layers Using Spin Torque from the Spin Hall Effect, Phys. Rev. Lett. **109**, 096602 (2012).

[4] R. Dorrance, J. G. Alzate, S. S. Cherepov, P. Upadhyaya, I. N. Krivorotov, J. A. Katine, J. Langer, K. L. Wang, P. K. Amiri, and D. Marković, Diode-MTJ crossbar memory cell using voltage-induced unipolar switching for high-density MRAM, IEEE Electron Device Lett. **34**, 753 (2013).

[5] K. L. Wang, J. G. Alzate, and P. K. Amiri, Low-power nonvolatile spintronic memory: STT-RAM and beyond, J. Phys. D **46**, 7 (2013).

[6] S. Ikeda, K. Miura, H. Yamamoto, K. Mizunuma, H. D. Gan, M. Endo, S. Kanai, J. Hayakawa, F. Matsukura, and

H. Ohno, A perpendicular-anisotropy CoFeB-MgO magnetic tunnel junction, Nat. Mater. **9**, 721 (2010).

[7] S. Mangin, D. Ravelosona, J. A. Katine, M. J. Carey, B. D. Terris, and E. E. Fullerton, Current-induced magnetization reversal in nanopillars with perpendicular anisotropy, Nat. Mater. **5**, 210 (2006).

[8] X. Qiu, K. Narayanapillai, Y. Wu, P. Deorani, D. H. Yang, W. S. Noh, J. H. Park, K. J. Lee, H. W. Lee, and H. Yang, Spin-orbit-torque engineering via oxygen manipulation, Nat. Nanotechnol. **10**, 333 (2015).

[9] C. Zhang, S. Fukami, H. Sato, F. Matsukura, and H. Ohno, Spin-orbit torque induced magnetization switching in nanoscale Ta/CoFeB/MgO, Appl. Phys. Lett. **107**, 012401 (2015).

[10] G. Yu, L. T. Chang, M. Akyol, P. Upadhyaya, C. He, X. Li, K. L. Wong, P. K. Amiri, and K. L. Wang, Current-driven perpendicular magnetization switching in Ta/CoFeB/[TaOx or MgO/TaOx] films with lateral structural asymmetry, Appl. Phys. Lett. **105**, 102411 (2014).

[11] C. O. Avci, K. Garello, C. Nistor, S. Godey, B. Ballesteros, A. Mugarza, A. Barla, M. Valvidares, E. Pellegrin, A. Ghosh, I. M. Miron, O. Boulle, S. Auffret, G. Gaudin, and P. Gambardella, Fieldlike and antidamping spin-orbit torques in as-grown and annealed Ta/CoFeB/MgO layers, Phys. Rev. B **89**, 214419 (2014).

[12] C. F. Pai, L. Liu, Y. Li, H. W. Tseng, D. C. Ralph, and R. A. Buhrman, Spin transfer torque devices utilizing the giant spin Hall effect of tungsten, Appl. Phys. Lett. **101**, 122404 (2012).

[13] M. Akyol, G. Yu, J. G. Alzate, P. Upadhyaya, X. Li, K. L. Wong, A. Ekicibil, P. K. Amiri, and K. L. Wang, Current-induced spin-orbit torque switching of perpendicularly magnetized HfCoFeB|MgO and Hf|CoFeB|TaOx structures, Appl. Phys. Lett. **106**, 162409 (2015).

[14] M. Akyol, J. G. Alzate, G. Yu, P. Upadhyaya, K. L. Wong, A. Ekicibil, P. K. Amiri, and K. L. Wang, Effect of the oxide layer on current-induced spin-orbit torques in HfCoFeB|MgO and Hf|CoFeB|TaOx structures, Appl. Phys. Lett. **106**, 032406 (2015).

[15] Y. Fan, P. Upadhyaya, X. Kou, M. Lang, S. Takei, Z. Wang, J. Tang, L. He, L. T. Chang, M. Montazeri, G. Yu, W. Jiang, T. Nie, R. N. Schwartz, Y. Tserkovnyak, and K. L. Wang, Magnetization switching through giant spin-orbit torque in a magnetically doped topological insulator heterostructure, Nat. Mater. **13**, 699 (2014).

[16] J. Kim, J. Sinha, M. Hayashi, M. Yamanouchi, S. Fukami, T. Suzuki, S. Mitani, and H. Ohno, Layer thickness dependence of the current-induced effective field vector in TaCoFeB|MgO, Nat. Mater. **12**, 240 (2013).

[17] L. Liu, T. Moriyama, D. C. Ralph, and R. A. Buhrman, Spin-Torque Ferromagnetic Resonance Induced by the Spin Hall Effect, Phys. Rev. Lett. **106**, 036601 (2011).

[18] K. Garello, I. M. Miron, C. O. Avci, F. Freimuth, Y. Mokrousov, S. Blügel, S. Auffret, O. Boulle, G. Gaudin, and P. Gambardella, Symmetry and magnitude of spin-orbit torques in ferromagnetic heterostructures, Nat. Nanotechnol. **8**, 587 (2013).

[19] G. Yu, P. Upadhyaya, Y. Fan, J. G. Alzate, W. Jiang, K. L. Wong, S. Takei, S. A. Bender, L. T. Chang, Y. Jiang, M. Lang, J. Tang, Y. Wang, Y. Tserkovnyak, P. K. Amiri, and K. L. Wang, Switching of perpendicular magnetization by spin-orbit torques in the absence of external magnetic fields, Nat. Nanotechnol. **9**, 548 (2014).

[20] G. Yu, M. Akyol, P. Upadhyaya, X. Li, C. He, Y. Fan, M. Montazeri, J. G. Alzate, M. Lang, K. L. Wong, P. K. Amiri, and K. L. Wang, Competing effect of spin-orbit torque terms on perpendicular magnetization switching in structures with multiple inversion asymmetries, Sci. Rep. **6**, 23956 (2016).

[21] J. Torrejon, F. Garcia-Sanchez, T. Taniguchi, J. Sinha, S. Mitani, J. V. Kim, and M. Hayashi, Current-driven asymmetric magnetization switching in perpendicularly magnetized CoFeB/MgO heterostructures, Phys. Rev. B **91**, 214434 (2015).

[22] A. v. d. Brink, G. Vermijs, A. Solignac, J. Koo, J. T. Kohlhepp, H. J. M. Swagten, and B. Koopmans, Field-free magnetization reversal by spin-Hall effect and exchange bias, Nat. Commun. **7**, 10854 (2016).

[23] S. Fukami, C. Zhang, S. DuttaGupta, A. Kurenkov, and H. Ohno, Magnetization switching by spin-orbit torque in an antiferromagnet-ferromagnet bilayer system, Nat. Mater. **15**, 535 (2016).

[24] Y. C. Lau, D. Betto, K. Rode, J. M. D. Coey, and P. Stamenov, Spin-orbit torque switching without an external field using interlayer exchange coupling, Nat. Nanotechnol. **11**, 758 (2016).

[25] Y. W. Oh, S. C. Baek, Y. M. Kim, H. Y. Lee, K. D. Lee, C. G. Yang, E. S. Park, K. S. Lee, K. W. Kim, G. Go, J. R. Jeong, B. C. Min, H. W. Lee, K. J. Lee, and B. G. Park, Field-free switching of perpendicular magnetization through spin-orbit torque in antiferromagnet/ferromagnet/oxide structures, Nat. Nanotechnol. **11**, 858 (2016).

[26] J. Nogués and I. K. Schuller, Exchange bias, J. Magn. Magn. Mater. **192**, 203 (1999).

[27] M. Hayashi, J. Kim, M. Yamanouchi, and H. Ohno, Quantitative characterization of the spin-orbit torque using harmonic Hall voltage measurements, Phys. Rev. B **89**, 144425 (2014).

[28] M. Yang, K. Cai, H. Ju, K. W. Edmonds, G. Yang, S. Liu, B. Li, B. Zhang, Y. Sheng, S. Wang, Y. Ji, and K. Wanga, Spin-orbit torque in Pt/CoNiCo/Pt symmetric devices, Sci. Rep. **6**, 20778 (2016).

[29] S. Emori, U. Bauer, S. Woo, and G. S. D. Beach, Large voltage-induced modification of spin-orbit torques in Pt/Co/GdOx, Appl. Phys. Lett. **105**, 222401 (2014).

[30] D. Wu, G. Yu, C. T. Chen, S. A. Razavi, Q. Shao, X. Li, B. Zhao, K. L. Wong, C. He, Z. Zhang, P. K. Amiri, and K. L. Wang, Spin-orbit torques in perpendicularly magnetized Ir22Mn78/Co20Fe60B20/MgO multilayer, Appl. Phys. Lett. **109**, 222401 (2016).

[31] G. Yu, P. Upadhyaya, K. L. Wong, W. Jiang, J. G. Alzate, J. Tang, P. K. Amiri, and K. L. Wang, Magnetization switching through spin-Hall-effect-induced chiral domain wall propagation, Phys. Rev. B **89**, 104421 (2014).

[32] J.-C. Rojas-Sánchez, N. Reyren, P. Laczkowski, W. Savero, J.-P. Attané, C. Deranlot, M. Jamet, J.-M. George, L. Vila, and H. Jaffrès, Spin Pumping and Inverse Spin Hall Effect in Platinum: The Essential Role of Spin-Memory Loss at Metallic Interfaces, Phys. Rev. Lett. **112**, 106602 (2014).

[33] C. Binek, Training of the exchange-bias effect: A simple analytic approach, Phys. Rev. B **70**, 014421 (2004).

[34] M. Ali, C. H. Marrows, M. Al-Jawad, B. J. Hickey, A. Misra, U. Nowak, and K. D. Usadel, Antiferromagnetic layer thickness dependence of the IrMn/Co exchange-bias system, Phys. Rev. B **68**, 214420 (2003).

[35] H. Xi and R. M. White, Theory of the blocking temperature in polycrystalline exchange biased bilayers based on a thermal fluctuation model, J. Appl. Phys. **94**, 5850 (2003).

[36] S. Maat, K. Takano, S. S. P. Parkin, and E. E. Fullerton, Perpendicular Exchange Bias of Co/Pt Multilayers, Phys. Rev. Lett. **87**, 087202 (2001).

[37] A. Hochstrat, C. Binek, and W. Kleemann, Training of the exchange-bias effect in NiO-Fe heterostructures, Phys. Rev. B **66**, 092409 (2002).

[38] K. Zhang, T. Zhao, and H. Fujiwara, Training effect of exchange biased iron-oxide/ferromagnet systems, J. Appl. Phys. **89**, 6910 (2001).

[39] P. Miltényi, M. Gierlings, J. Keller, B. Beschoten, G. Güntherodt, U. Nowak, and K. D. Usadel, Diluted Antiferromagnets in Exchange Bias: Proof of the Domain State Model, Phys. Rev. Lett. **84**, 4224 (2000).

[40] T. Gredig, I. N. Krivorotov, and E. D. Dahlberg, Magnetization reversal in exchange biased Co/CoO probed with anisotropic magnetoresistance, J. Appl. Phys. **91**, 7760 (2002).

[41] F. Radu, M. Etzkorn, R. Siebrecht, T. Schmitte, K. Westerholt, and H. Zabel, Interfacial domain formation during magnetization reversal in exchange-biased Co/CoO bilayers, Phys. Rev. B **67**, 134409 (2003).

[42] T. Hauet, J. A. Borchers, P. Mangin, Y. Henry, and S. Mangin, Training Effect in an Exchange Bias System: The Role of Interfacial Domain Walls, Phys. Rev. Lett. **96**, 067207 (2006).

[43] S. Brems, K. Temst, and C. V. Haesendonck, Origin of the Training Effect and Asymmetry of the Magnetization in Polycrystalline Exchange Bias Systems, Phys. Rev. Lett. **99**, 067201 (2007).